Journal of Solid Mechanics Vol. 11, No. 4 (2019) pp. 759-777
DOI: 10.22034/jsm.2019.668611

Pull-In Instability of MSGT Piezoelectric Polymeric FG-SWCNTs Reinforced Nanocomposite Considering Surface Stress Effect

A. GhorbanpourArani [1,2 *], B. Rousta Navi [1], M. Mohammadimehr [1], S. Niknejad[1], A.A. Ghorbanpour Arani[3],A. Hosseinpour [4]

[1]*Department of Solid Mechanics, Faculty of Mechanical Engineering, University of Kashan, Kashan, Iran*
[2]*Institute of Nanoscience & Nanotechnology, University of Kashan, Kashan, Iran*
[3]*School of Mechnical Engineering, College of Engineering, University of Tehran, Tehran, Iran*
[4]*Department of Mechanical Engineering and Engineering Science, University of North Carolina at Charlotte, USA*

Received 15 July 2019; accepted 17 September 2019

ABSTRACT

In this paper, the pull-in instability of piezoelectric polymeric nanocomposite plates reinforced by functionally graded single-walled carbon nanotubes (FG-SWCNTs) based on modified strain gradient theory (MSGT) is investigated. Various types of SWCNTs are distributed in piezoelectric polymeric plate and surface stress effect is considered in this research. The piezoelectric polymeric nanocomposite plate is subjected to electro-magneto-mechanical loadings. The nonlinear governing equations are derived from Hamilton's principle. Then, pull-in voltage and natural frequency of the piezoelectric polymeric nanocomposite plates are calculated by Newton-Raphson method. There is a good agreement between the obtained and other researcher results. The results show that the pull-in voltage and natural frequency increase with increasing of applied voltage, magnetic field, FG-SWCNTs orientation angle and small scale parameters and decrease with increasing of van der Waals and Casimir forces, residual surface stress constant. Furthermore, highest and lowest pull-in voltages are belonging to FG-X and FG-O distribution types of SWCNTs.

Keywords: Pull-in instability; Piezoelectric polymeric nanocomposite plates; Surface stress effect; Modified strain gradient theory (MSGT).

1 INTRODUCTION

INVESTIGATION of pull-in phenomena is very important in micro and nano electro-mechanical systems (MEMS and NEMS). As the applied voltage is greater than pull-in voltage, there isn't any equilibrium of system and flexible electrode can be moved and bonded to fixed electrode then short circuiting occurs. This phenomenon is observed in various applications as: micro- accelerometer [1], actuator [2, 3], nanoswitch [4], capacitor [5], nano resonators [6], NEM smart sensors and transistor, micro and nano controllers, micro and nano resistors [7, 8],

*Corresponding author. Tel.: +98 31 55912450; Fax: +98 31 55912424.
E-mail address: aghorban@kashanu.ac.ir (A. Ghorbanpour Arani).

measurement devices and so on. In addition, the piezoelectric polymeric nanocomposite plate can be used these devices and improved the pull-in stability of them. Many researchers have interested to study the pull-in stability of MEMS. A size-dependent pull-in phenomenon in electrically actuated nanobeams including surface energies is modeled by Fu and Zhang [9]. Their results revealed that nanobeam becomes softer in higher applied voltage and lower thickness. Furthermore, the size effect on the pull-in stability for 'Si' beam and 'Al' beam is considerable in beam thickness smaller than 10 nm and 100 nm, respectively. Mohammadimehr et al. [10] presented the vibration analysis of a double-bonded nanocomposite piezoelectric plate reinforced by a boron nitride nanotube based on modified couple stress theory (MCST) under electro-thermo-mechanical loadings. They concluded that the natural frequency increases with an increase in the material length scale parameter. Wang et al [11] studied the static and vibrational behaviors of a multi-layer electromechanical-coupled microbeam based on the geometrically nonlinear theory of Euler– Bernoulli beams under axial extension. They concluded that pull-in voltage increases with increasing of pre-stress and dielectric thickness and decreases with an increase in the beam length. Stephan et al. [12] computed the pull-in curves for electrostatically actuated microsystems. They extended staggered and monolithic approaches for static pull-in stability. Analytical closed-form solutions for size-dependent static pull-in behavior in electrostatic micro-actuators via Fredholm integral equation is presented by Rudolf et al. [13]. They observed that pull-in behavior is more influenced by the small-scale parameter especially in clamped-clamped micro-beams. Their solution of the model of beam-type micro and nanoscale electrostatic actuators is explained by Duan et al. [14]. They proposed a new modified Adomian decomposition method for nonlinear boundary value problems. Mousavi et al. [15] explored the effect of small scale on the pull-in instability of nano-switches using DQM subjected to electrostatic and intermolecular forces using Eringen's nonlocal elasticity theory and Euler–Bernoulli beam model. They illustrated that for cantilever nano-beam, the nonlocal parameter has reduction effect on pull-in voltage whereas the critical deflection decreases with increasing of the nonlocal parameter and vice versa for clamped–clamped nano-beam. Furthermore, the deflection is more affected by the Casimir force than van der Waals (vdW) force at the same nonlocal parameter value. Dynamic pull-in instability of vibrating nano-actuators in the presence of actuation voltage including fringing field effect is presented by Sedighi et al. [16]. They showed that as the initial vibration amplitude increases, the pull-in voltage and fundamental frequency of nanobeam decrease. Influence of surface energy on the non-linear pull-in instability of nano-switches using geometrically non-linear Euler–Bernoulli beam theory is found by Wang and its co-worker [17]. They concluded that the Casimir force effect on the pull-in voltage is negligible in higher initial gap. Furthermore, the pull-in voltage decreases with increasing of length beam and the surface energy effect on the pull-in voltage increases with increasing of length of the beam and decreasing of height of beam. Non-linear behaviors of carbon nanotubes under electrostatic actuation based on strain gradient theory examined by Fakhrabadi et al. [18]. Their results showed that vdW force effect on the pull-in voltage of CNTs cannot be ignored. Also the pull-in voltage of CNTs increases with an increase in small scale parameters. The effect of a liquid layer, water, underneath an electrostatic nano actuator on the pull-in instability of actuator is presented by Yazdanpanahi et al. [19]. They used the modified Adomian decomposition method (MADM) to find an analytical solution for bucking and pull-in instability of the actuator. In addition, they introduced balance liquid layer (BLL) value in which maximum deflection at the onset of pull-in instability does not change with variation of the Casimir force. Size-dependent stability of a fully clamped micro-electro-mechanical beam under shock acceleration pulse based on the MCST and Euler–Bernoulli beam model is extended by Askari and Tahani [20]. They determined that the small-scale effect on dynamic pull-in voltage can be neglected as thickness to the material length scale parameter ratio is greater than 15. The effects of van der Waals and Casimir forces on the static deflection and pull-in instability of a micro/nano cantilever gyroscope with a mass at its end is investigated by Mojahedi et al. [21]. They depicted that the static deflection decreases with increasing of van der Waals and Casimir forces in the vicinity of the pull-in instability. The thermal effect on the pull-in instability of functionally graded Euler–Bernoulli micro-beams under the combined electrostatic force, temperature change and Casimir force is studied by Jia et al. [22]. They found that the pull-in voltage increases with an increase in volume fraction of micro-beams and rising of temperature. Juillard [23] obtained resonant pull-in of micro- electromechanical oscillators. He established it for parallel-plate resonator and then extended to clamped–clamped and cantilever beams. Huang et al. [24] presented an exact model to obtain the pull-in voltage of micro cantilever beams under tilted and curled effects. They suggested a modified deformation function to compute the pull-in voltage of the suspended cantilever beam with residual deformations. Wang et al. [25] investigated the effects of surface energy on the pull-in instability and free vibration of electrostatically actuated micro/nanoscale using MCST. They solved governing equations with a reduced-order model and the displacement iteration pull-in extraction (DIPIE) algorithm. Their results demonstrated that the pull-in voltage and fundamental frequency of the plate are considerably improved by the material length scale, surface energy and geometrically nonlinear deformation. Rahaeifard and Ahmadian [26] carried out the static deflection and pull-in instability of electrostatically actuated micro cantilever beam based on MSGT and classical

plate theory. They showed that the classical plate theory underestimates the stiffness. The pull-in instability of nano-actuated Euler–Bernoulli beams made of nanocrystalline silicon (Nc–Si) under distributed electrostatic force based on MCST using a finite difference-based solution is studied by Shaat and Abdelkefi [27]. They illustrated that surface energy has important effects on the pull-in voltage of the actuators. Pull-in voltage analysis of the fixed-fixed microbeam with piezoelectric layers is performed by Xiao et al. [28]. They concluded that the size effect becomes significant if the dimension of micro beam is comparable to the material length scale parameter. The dynamic pull-in instability and snap-through analysis of initially curved microbeams is performed by Moghimi Zand [29]. He found that the pull-in instability increases by increasing initial relative elevation h. Ghorbanpour Arani et al. [30, 31] investigated nonlinear pull-in instability of nano-switches considering electrostatic and Casimir forces using nonlocal theory. Their results indicated that the pull-in voltage increases with increasing of the gap value and the nonlocal parameter. Coupled mechanism and pull-in instability of several probe-membrane assemblies subjected to electrostatic force is done by Lin and Lee [32]. They indicated that the larger the membrane tension and beam bending rigidity are lead to the higher the pull-in voltage. The electromechanical coupling behaviors of carbon nanotubes (CNTs) reinforced cantilever nano-actuator is performed by Yang et al. [33]. They concluded that the pull-in deflection of carbon nanotubes reinforced cantilever nanobeam decreases with an increase in applied voltage. Furthermore, the pull-in voltage and pull-in deflection of carbon nanotubes (CNTs) reinforced cantilever nano-actuator more decrease with increasing of Casimir force than that of van der Waals force. Additionally, pull-in voltage increases with increasing of the nonlocal parameter and vice versa for the pull-in deflection. Tajalli et al. [34] examined dynamic pull-in behavior of microplates actuated by a suddenly applied electrostatic force based on first-order shear deformation plate (FSDT) and classical plate theories (CPT) using finite element method. As the thickness of microplate decreases, the dynamic responses of CPT are deferent from FSDT. On the pull-in instability of double-walled carbon nanotube-based nano electromechanical systems with cross-linked walls is investigated by Fakhrabadi et al. [35]. Keivani et al. [36] developed a size-dependent model for instability analysis of paddle-type and double-sided NEMS measurement sensors in the presence of centrifugal force. They concluded that the vdW attraction decreases the pull-in voltage of sensor while the size effect increases it. Talebian et al. [37] presented effect of temperature on pull-in voltage and natural frequency of an electrostatically actuated microplate. They illustrated that the pull-in voltage and first natural frequency decrease with increasing of the compressive residual stresses and positive changes of operating temperature. The nonlinear pullout response of fiber-reinforced-polymer (FRP) ground anchors using an analytical transfer matrix method is anticipated by Zheng and Dai [38]. Mohammadimehr and Salemi [39] developed strain gradient theory (SGT) for bending and buckling analysis of FG mindlin nanoplate. They concluded that considering SGT leads to increase stiffness of nanoplate. Surface stress effect on the pull-in instability of hydrostatically and electrostatically actuated circular nanoplates using the generalized differential quadrature is investigated by Ansari et al. [40]. They concluded that by considering surface effect, the pull-in instability occurs at higher applied voltages for lower thicknesses of nanoplates. Also the pull-in voltage of simply-supported is smaller than that of for clamped nanoplates and pull-in voltage decreases with an increase in the thickness of plate. The size-dependent pull-in instability of geometrically non-linear rectangular nanoplates including surface stress effects under hydrostatic and electrostatic actuations using the generalized differential quadrature and a non-classical continuum plate model is carried out by Ansari et al. [41]. They concluded that in the smaller thicknesses of the nanoplates, the result of pull-in voltages in classical model is lower than those of in a non-classical model. Mohammadimehr et al. [42] investigated vibration of viscoelastic piezoelectric polymeric nanocomposite plate reinforced by FG-SWCNTs using meshless method based on MSGT and MSCT. Mao et al. [43] used the 'equal area method' to investigate the load carrying capacity of circular sandwich plates (two metallic face-sheets adhered to a metallic foam-core) subjected to transverse quasi-static point central loading, and the plates are simply supported or fully clamped at the edges. Ghorbanpour Arani et al. [44] investigated surface stress and agglomeration effects on nonlocal biaxial buckling polymeric nanocomposite plate reinforced by CNT based on nonlocal theory. In another work, they used a new trigonometric higher order shear deformation plate theory for smart vibration control of magnetostrictive nano-plate based on nonlocal theory [45]. Surface stress effect on the nonlocal biaxial buckling and bending analysis of polymeric piezoelectric nanoplate reinforced by CNT using Eshelby-Mori-Tanaka approach is performed by Mohammadimehr et al. [46]. Size dependent pull-in instability of functionally graded sandwich nanobridges using higher order shear deformation theory subjected to electrostatic actuation effect and intermolecular Casimir forces is carried out by Shojaeian1 and Zeighampour [47]. They used the modified couple stress theory to consider size dependent effect. They revealed that the modified couple stress theory leads to precise pull-in results with respect to experimental results. Also considering the Casimir force in low gap distances and high lengths have an important role in the pull-in instability. Yang et al. [48] performed analytical analysis of pull-in instability of carbon nanotube-reinforced nano-switches considering scale, surface and thermal effects. They concluded that Casimir force in macro effects has larger

influences on the pull-in voltage than that of van der Waals force. Dynamic stability of modified strain gradient theory sinusoidal viscoelastic piezoelectric polymeric functionally graded single-walled carbon nanotubes reinforced nanocomposite plate considering surface stress and agglomeration effects under hydro-thermo-electro-magneto-mechanical loadings is extended by Mohammadimehr et al. [49]. Free vibration behavior of functionally graded carbon nanotube-reinforced composite (FG-CNTRC) cylindrical panel embedded in piezoelectric layers is investigated by Alibeigloo [50]. They considered various distribution types of SWCNTS. Dynamic instability analysis of doubly clamped cylindrical nanowires in the presence of Casimir attraction and surface effects using modified couple stress theory is performed by Sedighi and Bozorgmehri [51]. Exact solution for axial and transverse dynamic response of functionally graded nanobeam under moving constant load based on nonlocal elasticity theory is carried out by Hosseini and Rahmani [52]. They used the Laplace transform for the transverse and axial dynamic response. Zare [53] presented pull-in behavior analysis of vibrating functionally graded micro-cantilevers under suddenly DC voltage. Modified couple stress for the buckling of a nanoplate subjected to non-uniform compression based on the four-variable plate theory is developed by Malikan [53]. Ghorbanpour Arani et al. [54] examined sinusoidal surface couple stress theory for dynamic instability of visco-SWCNTs conveying pulsating fluid. They showed that the modified couple stress theory results is higher than the classical one. Magneto-electro-elastic dynamic analysis of microbeam using the Galerkin reduced order model is established by Amiri et al. [55]. Surface stress effect on the mechanical behavior of plate are seen in many researcher's work [56-60] but surface stress effect on the pull-in stability has not been observed in their works.

In this article, pull-in stability and vibration of piezoelectric polymeric nanocomposite reinforced by FG-SWCNTs is investigated. Various types of SWCNTs are distributed in piezoelectric polymeric plate and the surface stress effect is considered in this research. Modified strain gradient theory is used to considering small-scale effect. The piezoelectric polymeric nanocomposite plate is subjected to electro-magneto-mechanical loadings. Material properties are determined by the extended rule of mixture.

2 GEOMETRY AND MATERIAL PROPERTY DEFINITIONS

Fig. 1 shows the piezoelectric polymeric nanocompsite plate with length *a*, width *b* and height *h*. *X*, *Y* and *Z* coordinates are placed in right corner of the piezoelectric polymeric nanocomposite plate. The nanocomposite connected to fixed electrode via dielectric space. g_0 is the air initial gap. Aligned FG-SWCNTs are longitudinally distributed in the piezoelectric polymeric nanocomposite plate. According to this figure, different distribution types of SWCNTs are assumed as uniform distribution (UD), *FG-O, FG-X* and *FG-V*. Volume fraction for four distribution types can be expressed as follows [42]:

$$VF_{SWCNT} = \begin{cases} VF^*_{SWCNT} \; Uiform \;\; Distribution \; (UD) \\ VF^*_{SWCNT} \left(1 + 2Z \;/ h\right) \qquad FG - V \\ 2VF^*_{SWCNT} \left(1 - 2|Z|/h\right) \qquad FG - O \\ 2VF^*_{SWCNT} \left(2|Z|/h\right) \qquad FG - X \end{cases} \tag{1}$$

where, VF^*_{SWCNT} is volume fraction of carbon nanotubes. The extended mixture of rule [44] is used to estimate the material properties of the piezoelectric polymeric nanocomposite plate as:

$$\begin{aligned} E_{11} &= \eta_1 VF_{SWCNT} E_{11}^{SWCNT} + VME_{11}^{M} \\ \frac{\eta_2}{E_{22}} &= \frac{VF_{SWCNT}}{E_{22}^{SWCNT}} + \frac{VM}{E_{22}^{M}} \\ \frac{\eta_3}{G_{12}} &= \frac{VF_{SWCNT}}{G_{12}^{SWCNT}} + \frac{VM}{G_{12}^{M}} \end{aligned} \tag{2}$$

where E_{11}^{SWCNT}, E_{22}^{SWCNT}, E_{11}^{M}, E_{22}^{M}, G_{12}^{SWCNT} and G_{12}^{M} denote longitudinal, transversely elastic and shear moduli of SWCNT and polymeric matrix, respectively. VM is volume fraction of matrix. η_1, η_2 and η_3 are constants which are define by dynamic molecule simulation.

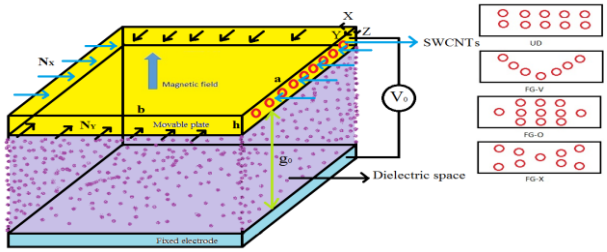

Fig.1
Schematic of functionally graded carbon nanotube reinforced piezoelectric polymeric nanocomposit plate switch.

3 FORMULATION OF THE PIEZOELECTRIC POLYMERIC NANOCOMPOSITE SWITCH

Based on CPT, as the middle plane displacements are assumed zero, strain-displacement relations can be expressed as follows:

$$\begin{Bmatrix} U(X,Y,Z) \\ V(X,Y,Z) \\ W(X,Y,Z) \end{Bmatrix} = \begin{Bmatrix} -Z\dfrac{\partial W(X,Y)}{\partial X} \\ -Z\dfrac{\partial W(X,Y)}{\partial Y} \\ W(X,Y) \end{Bmatrix} \tag{3}$$

$$\begin{Bmatrix} \varepsilon_{XX} \\ \varepsilon_{YY} \\ \varepsilon_{XY} \\ \varepsilon_{YZ} \\ \varepsilon_{XZ} \end{Bmatrix} = -Z \begin{Bmatrix} \dfrac{\partial^2 W(X,Y)}{\partial X^2} \\ \dfrac{\partial^2 W(X,Y)}{\partial Y^2} \\ \dfrac{\partial^2 W(X,Y)}{\partial X\,\partial Y} \\ 0 \\ 0 \end{Bmatrix} \tag{4}$$

Using piezoelectric constitutive equations [44], strain–stress relations can be written as follows:

$$\begin{Bmatrix} \sigma_{XX} \\ \sigma_{YY} \\ \sigma_{XY} \\ \sigma_{YZ} \\ \sigma_{XZ} \\ D_X \\ D_Y \\ D_Z \end{Bmatrix} = \begin{bmatrix} C_{11} & C_{12} & 0 & 0 & 0 & 0 & 0 & e_{13} \\ C_{12} & C_{22} & 0 & 0 & 0 & 0 & 0 & e_{23} \\ 0 & 0 & C_{66} & 0 & 0 & 0 & 0 & 0 \\ 0 & 0 & 0 & C_{44} & 0 & 0 & e_{24} & 0 \\ 0 & 0 & 0 & 0 & C_{55} & e_{15} & 0 & 0 \\ 0 & 0 & 0 & 0 & e_{15} & \xi_{11} & 0 & 0 \\ 0 & 0 & 0 & e_{24} & 0 & 0 & \xi_{22} & 0 \\ e_{13} & e_{23} & 0 & 0 & 0 & 0 & 0 & \xi_{33} \end{bmatrix} \begin{Bmatrix} \varepsilon_{XX} \\ \varepsilon_{YY} \\ \varepsilon_{XY} \\ \varepsilon_{YZ} \\ \varepsilon_{XZ} \\ -\dfrac{\partial \varphi}{\partial X} \\ -\dfrac{\partial \varphi}{\partial Y} \\ -\dfrac{\partial \varphi}{\partial Z} \end{Bmatrix} \tag{5}$$

where C_{ij}, e_{ij}, ξ_{ii} and φ are stiffness matrix, piezoelectric, dielectric coefficients and electrical potential, respectively which defined by the following equation [44]:

$$\varphi(X,Y,Z,t) = -\cos(\pi Z/h)\phi(X,Y,t) + 2ZV_0 e^{i\omega t}/h \tag{6}$$

where V_0 , ω, and t are the applied voltage and natural frequency, and time, respectively.

If FG-SWCNTs in the nanocomposite plate have angle θ, stiffness matrix, piezoelectric and dielectric coefficients change as follows [44]:

$$C^{'} = TCT^{-1}, e^{'} = T\,\mathrm{e}T^{-1}, \xi^{'} = T\,\zeta T^{-1} \tag{7}$$

where *R* is the rotation matrix that is considered as the following form [44]:

$$T = \begin{bmatrix} \cos^2(\theta) & \sin^2(\theta) & 0 & 0 & -2\cos(\theta)\sin(\theta) \\ \cos^2(\theta) & \sin^2(\theta) & 0 & 0 & 2\cos(\theta)\sin(\theta) \\ 0 & 0 & \cos(\theta) & \sin(\theta) & 0 \\ 0 & 0 & -\sin(\theta) & \cos(\theta) & 0 \\ \cos(\theta)\sin(\theta) & \cos(\theta)\sin(\theta) & 0 & 0 & \cos^2(\theta)-\sin^2(\theta) \end{bmatrix} \tag{8}$$

Variation form of Hamilton's principle can be stated as follows:
In presence of Casimir force:

$$\int_{t_1}^{t_2} \left(\delta K + \delta V_{f_l} + \delta V_f + \delta V_{Casimir} + \delta V_{elect} + \delta V_p - \delta U \right) dt = 0 \tag{9a}$$

In presence of *vdW* force:

$$\int_{t_1}^{t_2} \left(\delta K + \delta V_{f_l} + \delta V_f + \delta V_{VdW} + \delta V_{elect} + \delta V_p - \delta U \right) dt = 0 \tag{9b}$$

where δK and δU are the variations of kinetic energy, and strain energy, respectively. Also, δV_{f_l} , δV_f , $\delta V_{Casimir}$, δV_{VdW} , δV_{elect} , and δV_p are work done by Lorentz forces, elastic foundation forces, Casimir forces, van der Waals force, electrostatic force, and compression or tension loading, respectively ,variation of kinetic energy considering surface stress effect is determined as follows [44]:

$$\begin{aligned} \delta K = & \int_V \rho \left(\frac{\partial U}{\partial t}\frac{\partial \delta U}{\partial t} + \frac{\partial V}{\partial t}\frac{\partial \delta V}{\partial t} + \frac{\partial W}{\partial t}\frac{\partial \delta W}{\partial t} \right) dV = \int_V \left(\left[Z^2 \frac{\partial^4 W}{\partial X^2 \partial t^2} + Z^2 \frac{\partial^4 W}{\partial Y^2 \partial t^2} - \frac{\partial^2 W}{\partial t^2} \right] \delta W \right) \rho dZdA + \\ & \int_A \rho_s \left(\frac{\upsilon \rho_s h^2}{6(1-\upsilon)} \left(\frac{\partial^4 W}{\partial t^2 \partial X^2} + \frac{\partial^4 W}{\partial t^2 \partial Y^2} \right) \delta w + 2(b+h) \frac{\partial^2 W}{\partial t^2} \delta W \right) dA \end{aligned} \tag{10}$$

where ρ is the density of piezoelectric polymeric nanocomposite plate.

According to Ghorbanpour Arani et al. [44], variation of Lorentz forces due to the magnetic field in the direction of thickness can be obtained as follows:

$$\begin{aligned} \delta V_{f_l} = & \int_V \left(f_{Xl} \delta U + f_{Yl} \delta V \right) dV = \int_A \left(\left[\frac{\partial^2 U}{\partial X^2} + \frac{\partial^2 V}{\partial X\, \partial Y} + \frac{\partial^2 U}{\partial Z^2} \right] \delta U + \left[\frac{\partial^2 V}{\partial X^2} + \frac{\partial^2 U}{\partial X\, \partial Y} + \frac{\partial^2 V}{\partial Z^2} \right] \delta V \right) \eta H_Z^2 \, dZdA \\ = & -\int_A \left(+ \left[Z^2 \nabla^4 W \right] \partial W \right) \eta H_Z^2 \, dZdA \end{aligned} \tag{11}$$

where H_Z and η denote magnetic field and the magnetic permittivity, respectively.

The nanocomposite plate is subjected to electrostatic forces with fringing effect and compression loadings. The works done by these external loads per unit area are defined as follows [56-58]:

$$\begin{aligned}\delta V_{elect} &= -\int_A \left(\frac{b\varepsilon_0 V_0^{\,2}}{2\left(g_0 - W\right)^2}\left[1+\hat{f}\,\frac{g_0 - W}{b}\right]\right)\delta W dA \\ &= -\int_A \left(\frac{b\varepsilon_0 V_0^{\,2}}{2g_0^{\,2}}\left[\begin{array}{l} 1+\frac{\hat{f}g_0}{b}+\left(2+\frac{\hat{f}g_0}{b}\right)\left(\frac{W}{g_0}\right)+\left(3+\frac{\hat{f}g_0}{b}\right)\left(\frac{W}{g_0}\right)^2 \\ +\left(4+\frac{g_0\hat{f}}{b}\right)\left(\frac{W}{g_0}\right)^3+\left(5+\frac{g_0\hat{f}}{b}\right)\left(\frac{W}{g_0}\right)^4+\ldots \end{array}\right]\right)\delta W dA\end{aligned} \tag{12}$$

$$\delta V_{VdW} = -\int_A \left(\frac{Ab}{6\pi\left(g_0 - W\right)^3}\right)\delta W dA = -\int_A \frac{Ab}{6\pi g_0^{\,3}}\left(\begin{array}{l} 1+3\left(\frac{W}{g_0}\right)+6\left(\frac{W}{g_0}\right)^2 \\ +10\left(\frac{W}{g_0}\right)^3+15\left(\frac{W}{g_0}\right)^4+\ldots \end{array}\right)\delta W dA \tag{13}$$

$$\delta V_{Casimir} = -\int_A \left(\frac{\pi^2 hcb}{240\left(g_0 - W\right)^4}\right)\delta W dA = -\int_A \frac{\pi^2 hcb}{240 g_0^{\,4}}\left(\begin{array}{l} 1+4\left(\frac{W}{g_0}\right)+10\left(\frac{W}{g_0}\right)^2 \\ +20\left(\frac{W}{g_0}\right)^3+35\left(\frac{W}{g_0}\right)^4+\ldots \end{array}\right)\delta W dA \tag{14}$$

Work done by the other forces can be stated as follows:

$$\delta V_p = \int_A \left(N_X \frac{\partial^2 W}{\partial X^2} + N_Y \frac{\partial^2 W}{\partial Y^2} + 2e_{13}V_0 \frac{\partial^2 W}{\partial X^2} + 2e_{23}V_0 \frac{\partial^2 W}{\partial Y^2}\right)\delta W dA \tag{15}$$

where A, h and c are constants of Humaker, Plank and the light speed in vacuum, respectively. The above expression, with small displacement assumption and using the expansion of $\frac{1}{1-z} = 1+z+z^2+\ldots$ are simplified. It can be mentioned that Casimir force appears in larger gap ($>10\mu m$) and van der Waals force emerges in smaller gap ($<10\mu m$) [56-58]. Variation of strain energy considering surface stress effect can be stated as follows:

$$\begin{aligned}\delta U = &\int_V \left(\begin{array}{l} \sigma_{XX}\delta\varepsilon_X + \sigma_{YY}\delta\varepsilon_Y + 2\sigma_{XY}\delta\varepsilon_{XY} + p_X\delta\gamma_X + p_Y\delta\gamma_Y + p_Z\delta\gamma_Z \\ +m_{XX}\delta\chi_X + m_{YY}\delta\chi_Y + 2m_{XY}\delta\chi_{XY} + \tau_{XXX}\delta\eta^1_{XXX} + \\ 3\tau_{XXY}\delta\eta^1_{XXY} + 3\tau_{XXZ}\delta\eta^1_{XXZ} + 3\tau_{YYZ}\delta\eta^1_{YYZ} + 3\tau_{YYX}\delta\eta^1_{YYX} + \\ \tau_{YYY}\delta\eta^1_{YYY} + 3\tau_{XZZ}\delta\eta^1_{XZZ} + 3\tau_{YZZ}\delta\eta^1_{YZZ} + \tau_{ZZZ}\delta\eta^1_{ZZZ} + 6\tau_{XYZ}\delta\eta^1_{XYZ} \\ -D_X\delta E_X - D_Y\delta E_Y - D_Z\delta E_Z \end{array}\right)dV + \\ &\int_A \left(\begin{array}{l} -\frac{\upsilon\tau_s h^2}{6(1-\upsilon)}\nabla^4 W\,\delta W - 4\tau_s(b+h)\left(\frac{\partial^2 W}{\partial X^2}+\frac{\partial^2 W}{\partial Y^2}\right)\delta W + \\ \frac{\upsilon\rho_s h^2}{6(1-\upsilon)}\left(\frac{\partial^4 W}{\partial t^2\partial X^2}+\frac{\partial^4 W}{\partial t^2\partial Y^2}\right)\delta W \end{array}\right)dA\end{aligned} \tag{16}$$

where p_i , m_{ij} and τ_{ijk} denote higher-order stresses which are determined as the following equations:

$$p_i = 2Gl_0^2\gamma_i \qquad m_{ij} = 2Gl_2^2\chi_{ij} \qquad \tau_{ijk} = 2Gl_1^2\eta^1_{ijk} \tag{17}$$

where l_0 , l_1 and l_2 are the three small-scale parameters. γ_i , χ_{ij} and η^1_{ijk} are the dilatation gradient vector, the symmetric rotation gradient tensor and the deviatoric stretch gradient tensor, respectively, which are defined as follows:

$$\begin{aligned}
&\gamma_i = \varepsilon_{mm,i}\\
&\vartheta = \frac{1}{2}curl\left(u\right)\\
&\chi_{ij} = \frac{1}{2}\left(\vartheta_{i,j} + \vartheta_{j,i}\right)\\
&\eta^1_{ijk} = \frac{1}{3}\left(\varepsilon_{jk,i} + \varepsilon_{ki,j} + \varepsilon_{ij,k}\right) - \frac{1}{15}\left(\delta_{ij}\left(\varepsilon_{mm,k} + 2\varepsilon_{mk,m}\right)\right) - \frac{1}{15}\left(\delta_{jk}\left(\varepsilon_{mm,i} + 2\varepsilon_{mi,m}\right)\right) - \frac{1}{15}\left(\delta_{ki}\left(\varepsilon_{mm,j} + 2\varepsilon_{mj,m}\right)\right)
\end{aligned} \tag{18}$$

Substituting Eqs. (3) and (4) into Eq. (18) yields the following equation:

$$\begin{aligned}
&\gamma_X = \frac{\partial\varepsilon_{XX}}{\partial X} + \frac{\partial\varepsilon_{YY}}{\partial X} = -Z\left(\frac{\partial^3 W}{\partial X^3} + \frac{\partial^3 W}{\partial X\,\partial Y^2}\right), \qquad \gamma_Y = \frac{\partial\varepsilon_{XX}}{\partial Y} + \frac{\partial\varepsilon_{YY}}{\partial Y} = -Z\left(\frac{\partial^3 W}{\partial X^2\partial Y} + \frac{\partial^3 W}{\partial Y^3}\right),\\
&\gamma_Z = \frac{\partial\varepsilon_{XX}}{\partial Z} + \frac{\partial\varepsilon_{YY}}{\partial Z} = -\left(\frac{\partial^2 W}{\partial X^2} + \frac{\partial^2 W}{\partial Y^2}\right), \qquad \chi_{XX} = \frac{\partial^2 W}{\partial X\,\partial Y},\ \chi_{YY} = -\frac{\partial^2 W}{\partial X\,\partial Y}, \qquad \chi_{XY} = \frac{1}{2}\left(\frac{\partial^2 W}{\partial Y^2} - \frac{\partial^2 W}{\partial X^2}\right)
\end{aligned} \tag{19}$$

$$\begin{aligned}
&\eta^1_{XXX} = \frac{2}{5}\frac{\partial\varepsilon_{XX}}{\partial X} - \frac{1}{5}\frac{\partial\varepsilon_{YY}}{\partial X} - \frac{2}{5}\frac{\partial\varepsilon_{XY}}{\partial Y} = z\left(-\frac{2}{5}\frac{\partial^3 W}{\partial X^3} + \frac{3}{5}\frac{\partial^3 W}{\partial X\,\partial Y^2}\right)\\
&\eta^1_{XXY} = \eta^1_{YXX} = \eta^1_{XYX} = \frac{4}{15}\frac{\partial\varepsilon_{XX}}{\partial Y} + \frac{8}{15}\frac{\partial\varepsilon_{XY}}{\partial X} - \frac{1}{5}\frac{\partial\varepsilon_{YY}}{\partial Y} = z\left(-\frac{4}{5}\frac{\partial^3 W}{\partial Y\,\partial X^2} + \frac{1}{5}\frac{\partial^3 W}{\partial Y^3}\right)\\
&\eta^1_{XXZ} = \eta^1_{XZZ} = \eta^1_{XZX} = \frac{4}{15}\frac{\partial\varepsilon_{XX}}{\partial Z} - \frac{1}{15}\frac{\partial\varepsilon_{YY}}{\partial Z} = -\frac{4}{15}\frac{\partial^2 W}{\partial X^2} + \frac{1}{15}\frac{\partial^2 W}{\partial Y^2}\\
&\eta^1_{XYY} = \eta^1_{YYX} = \eta^1_{YXY} = \frac{4}{15}\frac{\partial\varepsilon_{YY}}{\partial X} + \frac{8}{15}\frac{\partial\varepsilon_{XY}}{\partial Y} - \frac{1}{5}\frac{\partial\varepsilon_{XX}}{\partial X} = z\left(-\frac{4}{5}\frac{\partial^3 W}{\partial X\,\partial Y^2} + \frac{1}{5}\frac{\partial^3 W}{\partial X^3}\right)\\
&\eta^1_{YYY} = \frac{2}{5}\frac{\partial\varepsilon_{YY}}{\partial Y} - \frac{1}{5}\frac{\partial\varepsilon_{XX}}{\partial Y} - \frac{2}{5}\frac{\partial\varepsilon_{XY}}{\partial X} = z\left(\frac{3}{5}\frac{\partial^3 W}{\partial Y\,\partial X^2} - \frac{2}{5}\frac{\partial^3 W}{\partial Y^3}\right)\\
&\eta^1_{YZZ} = \eta^1_{ZYZ} = \eta^1_{ZZY} = -\frac{2}{15}\frac{\partial\varepsilon_{XY}}{\partial X} - \frac{1}{15}\frac{\partial\varepsilon_{XX}}{\partial Y} - \frac{1}{5}\frac{\partial\varepsilon_{YY}}{\partial Y} = z\left(\frac{1}{5}\frac{\partial^3 W}{\partial Y\,\partial X^2} + \frac{1}{5}\frac{\partial^3 W}{\partial Y^3}\right)\\
&\eta^1_{YYZ} = \eta^1_{YZY} = \eta^1_{ZYY} = -\frac{1}{15}\frac{\partial\varepsilon_{XX}}{\partial Z} + \frac{4}{15}\frac{\partial\varepsilon_{YY}}{\partial Z} = -\frac{4}{15}\frac{\partial^2 W}{\partial Y^2} + \frac{1}{15}\frac{\partial^2 W}{\partial X^2}\\
&\eta^1_{XZZ} = \eta^1_{ZXZ} = \eta^1_{ZZX} = -\frac{1}{15}\frac{\partial\varepsilon_{YY}}{\partial X} - \frac{2}{15}\frac{\partial\varepsilon_{XY}}{\partial Y} - \frac{1}{5}\frac{\partial\varepsilon_{XX}}{\partial X} = z\left(\frac{1}{5}\frac{\partial^3 W}{\partial X^3} + \frac{1}{5}\frac{\partial^3 W}{\partial X\,\partial Y^2}\right)\\
&\eta^1_{ZZZ} = -\frac{1}{5}\left(\frac{\partial\varepsilon_{XX}}{\partial Z} + \frac{\partial\varepsilon_{YY}}{\partial Z}\right) = \frac{1}{5}\frac{\partial^2 W}{\partial X^2} + \frac{1}{5}\frac{\partial^2 W}{\partial Y^2}\\
&\eta^1_{XYZ} = \eta^1_{YZX} = \eta^1_{ZXY} = \eta^1_{ZYX} = \eta^1_{YXZ} = \eta^1_{XZY} = \frac{1}{3}\left(\frac{\partial\varepsilon_{XY}}{\partial Z}\right) = -\frac{1}{3}\frac{\partial^2 W}{\partial X\,\partial Y}
\end{aligned} \tag{20}$$

Substituting Eqs. (10)-(16), (19) and (20) in Eq. (9) and using Ref. [40] for surface stress effect, the motion equations can be defined as follows:

$$
\begin{aligned}
&I_1\frac{\partial^4 W}{\partial X^2\partial t^2}+I_1\frac{\partial^4 W}{\partial Y^2\partial t^2}-\left(I_2+\rho_s\left(b+h\right)\right)\frac{\partial^2 W}{\partial t^2}-\frac{\upsilon\rho_s h^2}{6(1-\upsilon)}\left(\frac{\partial^4 W}{\partial t^2\partial X^2}+\frac{\partial^4 W}{\partial t^2\partial Y^2}\right)=F\left(X,Y,V_0\right)=\\
&-\frac{b\varepsilon_0 V_0^2}{2g_0^2}\left[\begin{array}{l}1+\frac{g_0\hat{f}}{b}+\left(2+\frac{g_0\hat{f}}{b}\right)\left(\frac{W}{g_0}\right)+\left(3+\frac{g_0\hat{f}}{b}\right)\left(\frac{W}{g_0}\right)^2\\+\left(4+\frac{g_0\hat{f}}{b}\right)\left(\frac{W}{g_0}\right)^3+\left(5+\frac{g_0\hat{f}}{b}\right)\left(\frac{W}{g_0}\right)^4\end{array}\right]-\left(\frac{2e_{31}h}{\pi}\phi_{,XX}+\frac{2e_{32}h}{\pi}\phi_{,YY}\right)\\
&+P_1\nabla^4 W+D_{11}\frac{\partial^4 W}{\partial X^4}+2D_{12}\frac{\partial^4 W}{\partial Y^2\partial X^2}+D_{22}\frac{\partial^4 W}{\partial Y^4}+4D_{66}\frac{\partial^4 W}{\partial Y^2\partial X^2}-\frac{sAb}{6g_0^3}\left(\begin{array}{l}1+3\left(\frac{W}{g_0}\right)+6\left(\frac{W}{g_0}\right)^2\\+10\left(\frac{W}{g_0}\right)^3+15\left(\frac{W}{g_0}\right)^4\end{array}\right)\\
&-D_{33}\nabla^4 W-D_{44}\frac{2\partial^6 W}{5\partial X^6}-D_{44}\frac{2\partial^6 W}{5\partial Y^6}-\frac{6D_{44}}{5}\left(\frac{\partial^6 W}{\partial Y^4\partial X^2}+\frac{\partial^6 W}{\partial Y^2\partial X^4}\right)-N_X\frac{\partial^2 W}{\partial X^2}-N_Y\frac{\partial^2 W}{\partial Y^2}\\
&-\frac{r\pi^2 hcb}{240g_0^4}\left(\begin{array}{l}1+4\left(\frac{W}{g_0}\right)+10\left(\frac{W}{g_0}\right)^2\\+20\left(\frac{W}{g_0}\right)^3+35\left(\frac{W}{g_0}\right)^4\end{array}\right)+\frac{4D_{55}}{15}\left(\frac{\partial^4 W}{\partial Y^4}+\frac{\partial^4 W}{\partial X^4}\right)+\frac{8D_{55}}{15}\frac{\partial^4 W}{\partial Y^2\partial X^2}-2e_{13}V_0\frac{\partial^2 W}{\partial X^2}-2e_{23}V_0\frac{\partial^2 W}{\partial Y^2}\\
&-D_{77}\left(\frac{\partial^6 W}{\partial X^6}+\frac{3\partial^6 W}{\partial Y^4\partial X^2}+\frac{3\partial^6 W}{\partial Y^2\partial X^4}+\frac{\partial^6 W}{\partial Y^6}\right)+D_{88}\left(\frac{\partial^4 W}{\partial X^4}+\frac{2\partial^4 W}{\partial Y^2\partial X^2}+\frac{\partial^4 W}{\partial Y^4}\right)-\frac{\upsilon\tau_s h^2}{6(1-\upsilon)}\nabla^4 W\\
&-2\tau_s(b+h)\left(\frac{\partial^2 W}{\partial X^2}+\frac{\partial^2 W}{\partial Y^2}\right)+E_s(bh^2/2+h^3/6)\left(\frac{\partial^4 W}{\partial X^4}+\frac{\partial^4 W}{\partial Y^4}\right)
\end{aligned}
\tag{21}
$$

$$
\xi_{11}\frac{h}{2}\phi_{,XX}+\xi_{22}\frac{h}{2}\phi_{,YY}-2e_{31}\frac{h}{\pi}\frac{\partial^2 W}{\partial X^2}-2e_{32}\frac{h}{\pi}\frac{\partial^2 W}{\partial Y^2}-\frac{h}{2}\xi_{33}\phi=0 \tag{22}
$$

where ρ_s , E_s and τ_s are surface density, surface Lame and residual surface stress constants, respectively and thus we have:

$$
\begin{aligned}
&\left\{\begin{array}{l}I_1\\I_2\end{array}\right\}=\int_{-h/2}^{h/2}\left(\begin{array}{l}\rho Z^2\\\rho Z\end{array}\right)dZ,\left\{\begin{array}{l}D_{11}\\D_{12}\\D_{22}\\D_{66}\end{array}\right\}=\int_{-h/2}^{h/2}\left(\begin{array}{l}C_{11}\\C_{12}\\C_{22}\\C_{66}\end{array}\right)Z^2dZ\\
&\left\{\begin{array}{l}D_{33}\\D_{44}\\D_{55}\\D_{77}\\D_{88}\end{array}\right\}=\int_{-h/2}^{h/2}2\mu\left(\begin{array}{l}l_2^2\\l_1^2Z^2\\l_1^2\\l_0^2Z^2\\l_0^2\end{array}\right)dZ,P_1=\int_{-h/2}^{-h/2}H_Z^2\eta Z^2dz
\end{aligned}
\tag{23}
$$

In smaller gap, the Casimir force must be applied in Eq. (21), ($s=0, r=1$) and for smallest gap, the Van der Waals force is considered ($s=1, r=0$).

4 SOLVING METHODOLOGY

For solving of Eqs. (21) and (22), it is assumed $W\left(X,Y,t\right)=r\,w\left(X,Y\right)e^{i\omega t}$ and $\phi\left(X,Y,t\right)=\sin\left(m\pi X/a\right)\sin\left(n\pi Y/b\right)e^{i\omega t}$. $w\left(X,Y\right)$ is equal to $\sin\left(m\pi X/a\right)\sin\left(n\pi Y/b\right)$ for simply supported boundary conditions. ω is the natural frequency. It must be $\frac{\partial F\left(X,Y,V_0\right)}{\partial\delta}<0$ for stability of the piezoelectric polymeric nanocomposite plate and for the critical pull- in stability $\frac{\partial F\left(X,Y,V_0\right)}{\partial\delta}$ must be zero.

$$F\left(X,Y,V_0\right)=0:K_1+K_2r-K_3r+K_4r^2+K_5r^3+K_6r^4=0 \tag{24}$$

$$\frac{dF\left(X,Y,V_0\right)}{dr}=0:K_2-K_3+2K_4r+3K_5r^2+4K_6r^3=0 \tag{25}$$

where:

$$x=\frac{X}{a},y=\frac{Y}{b},\alpha=\frac{a}{b}$$

$$K_1=\int_0^1\int_0^1\phi_1\phi_2\left[\frac{b\varepsilon_0V_0^{\,2}}{2g_0^2}+\frac{sAb}{6g_0^3}+\frac{r\pi^2hcb}{240g_0^4}\right]\left(1/g_0D_{11}\right)dxdy$$

$$K_2=\int_0^1\int_0^1\phi_1^2\phi_2^2\left[\frac{2b\varepsilon_0V_0^{\,2}}{2g_0^2}+\frac{3sAb}{6g_0^3}+\frac{4r\pi^2hcb}{240g_0^4}\right]\left(1/g_0D_{11}\right)dxdy$$

$$K_3=\int_0^1\int_0^1\left[\begin{array}{l}\frac{d^4\phi_1}{dx^4}\phi_2^2\phi_1\left(P_1+D_{11}-D_{33}-\frac{\upsilon\tau_sh^2}{6(1-\upsilon)}+E_s(bh^2/2+h^3/6)+D_{88}+\frac{4D_{55}}{15}\right)+k_w\phi_1^2\phi_2^2+\frac{d^6\phi_2}{\alpha^6dy^6}\phi_1^2\phi_2\left(-\frac{2D_{44}}{5}-D_{77}\right)\\+2\frac{d^2\phi_1}{dx^2}\frac{d^2\phi_2}{\alpha^2dy^2}\phi_1\phi_2\left(P_1-\frac{\upsilon\tau_sh^2}{6(1-\upsilon)}+4D_{66}+D_{12}-D_{33}+D_{88}+\frac{4D_{55}}{15}\right)\\+\frac{d^4\phi_2}{\alpha^4dy^4}\phi_1^2\phi_2\left(P_1-\frac{\upsilon\tau_sh^2}{6(1-\upsilon)}+E_s(bh^2/2+h^3/6)+D_{22}-D_{33}+D_{88}+\frac{4D_{55}}{15}\right)+\frac{d^6\phi_1}{dx^6}\phi_1\phi_2^2\left(-\frac{2D_{44}}{5}-D_{77}\right)\\+\frac{d^2\phi_1}{dx^2}\phi_1\phi_2^2\left(-k_g-2\tau_s(b+h)-2e_{13}V_0-N_X\right)+\frac{d^2\phi_2}{\alpha^2dy^2}\phi_1^1\phi_2\left(-2\tau_s(b+h)-2e_{23}V_0-k_g-N_Y\right)\\+\frac{d^2\phi_1}{dx^2}\frac{d^4\phi_2}{dy^4}\phi_1\phi_2\left(-\frac{6D_{44}}{5}-3D_{77}\right)+\frac{d^4\phi_1}{dx^4}\frac{d^2\phi_2}{dy^2}\phi_1\phi_2\left(-\frac{6D_{44}}{5}-3D_{77}\right)\end{array}\right]\left(1/D_{11}\right)dxdy \tag{26}$$

$$K_4=\int_0^1\int_0^1\phi_1^3\phi_2^3\left[\frac{3b\varepsilon_0V_0^{\,2}}{2g_0^2}+\frac{6sAb}{6g_0^3}+\frac{10r\pi^2hcb}{240g_0^4}\right]\left(1/g_0D_{11}\right)dxdy$$

$$K_5=\int_0^1\int_0^1\phi_1^4\phi_2^4\left[\frac{4b\varepsilon_0V_0^{\,2}}{2g_0^5}+\frac{10sAb}{6g_0^3}+\frac{20r\pi^2hcb}{240g_0^4}\right]\left(1/g_0D_{11}\right)dxdy$$

$$K_6=\int_0^1\int_0^1\phi_1^5\phi_2^5\left[\frac{5b\varepsilon_0V_0^{\,2}}{2g_0^2}+\frac{15sAb}{6g_0^3}+\frac{35r\pi^2hcb}{240g_0^4}\right]\left(1/g_0D_{11}\right)dxdy$$

$$a_1=\frac{a^4b\varepsilon_0V_0^{\,2}}{2g_0^3D_{11}},a_3=\frac{a^4sAb}{6g_0^4D_{11}},a_4=\frac{a^4r\pi^2hcb}{240g_0^5D_{11}},a_5=\frac{N_xa^2}{D_{11}},a_6=\frac{N_ya^2}{D_{11}}$$

The Newton–Raphson method is a method for finding successively better approximations to the roots of function. It is one example of a root-finding algorithm for *f(x)=0*. The method begins with a function f defined over the numbers *x*, the function's derivative *f'*, and an initial guess x_0 for a root of the function *f*. If the function satisfies the assumptions made in the derivation of the formula and the initial guess is close, then a better approximation x_1 is x_0- *f(x0)/ f' (x0)*. The procedure is repeated as until a sufficiently accurate value is achieved. The transverse

displacement and pull-in voltage of the piezoelectric polymeric nanocomposite plate is calculated by solving of Eqs. (24) and (25) by Newton-Raphson method. The natural frequency of the piezoelectric polymeric nanocomposite plate is defined by replacing $W\left(X,Y,t\right)=A\ w\left(X,Y\right)e^{i\omega t}$ into Eqs. (21) and (22).

5 RESULTS AND DISCUSSIONS

The material properties and foundation parameters for the piezoelectric polymeric nanocomposite plate are listed in Table 1. At first time, the present results are validated by numerical results of Ref. [4] and then effects of pivotal parameters on the pull-in stability of the piezoelectric polymeric nanocomposite plate are investigated. The present and literature [4] results for pull-in voltage parameter ($a_1=V^2a^4/Dg^3$) of simply supported plate with various non-dimensional uniaxial loading ($a_2=N_xa/D$) are illustrated in Table 2. A good agreement is observed between these results and as non-dimensional uniaxial loading increases, the pull-in voltage parameter increases.

Table 3., shows the pull-in voltage parameter ($a_1=V^2a^4/Dg^3$) of simply supported piezoelectric polymeric nanocomposite plate reinforced by functionally graded SWCNTs for uniaxial compression ($N_Xa^2/D_{11}=10, N_Ya^2/\alpha^2D_{11}=0$) and biaxial compression ($N_Xa^2/D_{11}=10,\ N_Ya^2/\alpha^2D_{11}=10$). The results obtain for various distribution types of SWCNTs as: *UD*, *FG-V*, *FG-O* and *FG-X* based on classical theory (CT), $l=l_2=l_1=l_0=0$ and modified strain gradient theory (MSGT), $l=l_2=l_1=l_0\neq 0$. It is obvious that the biaxial compression loading in contrast to uniaxial compression loading, enriches the stiffness of the piezoelectric polymeric nanocomposite plate, consequently, the pull-in voltage parameter increases by increasing of these loads. Also, considering size effects leads to increase of the pull- in voltage parameter. Furthermore, among various distribution types of SWCNTs, *FG-O* and *FG-X* have the highest and lowest values for pull-in voltage parameter that means, the nanocomposite plate is more strengthened by FG-O SWCNTs than other distribution types of SWCNTs.

Table 1
The material properties and dimensions for the piezoelectric polymeric nanocomposite plate.[40]

Material properties		Dimension parameters	
VF_{SWCNT}	0.17	l_0	$5nm$
EM_{11}	8.3 *GPa*	l_1	$5nm$
ν_M	0.18	l_2	$5nm$
$E_{11SWCNT}$	5.6466 *TPa*	η	$4\pi e-7\ H/m$
$E_{22SWCNT}$	7.08 *TPa*	A	$[0.4,4]\times10^{-19}J$
$G_{12SWCNT}$	1.9445 *TPa*	c	$2.998\times10^8\ m/\sec$
ν_{SWCNT}	0.175	g_0	$1\mu m$
η_1	0.142	h	$(1.055/2\pi)\times10^{-34}J.\sec$
η_2	1.626	ε_0	$8.854\times10^{-12}C^2/N.m^2$
η_3	1.138	-	-
ρ_{SWCNT}	4000 kg/m^3	-	-
ρ_{SWCNT}	1750 kg/m^3	-	-

Table 2
Pull-in voltage ($a_1=V^2a^4/Dg^3$) of simply supported plate.

Non-dimensional axial loading ($a_2=N_xa/D$)	Zhang and Zhao [4]	Present work
5	52.18	55.14447
10	59.46	61.3434
15	66.74	67.5425
20	74.02	74.6940
25	81.29	82.446946
30	88.57	88.84032

Table 3
Pull-in voltage parameter ($a_1 = V^2 a^4 / D g^3$) of simply supported piezoelectric polymeric nanocomposite plate reinforced by functionally graded carbon nanotubes.

a/h	l/h	$N_X a^2/D_{11}=10, N_Y a^2/\alpha^2 D_{11}=0$				$N_X a^2/D_{11}=10, N_Y a^2/\alpha^2 D_{11}=0$			
		UD	*FG-V*	*FG-O*	*FG-X*	*UD*	*FG-V*	*FG-O*	*FG-X*
6	0	9.54	9.55	13.32	10.69	13.25	13.26	20.17	10.69
	0.1	9.59	9.59	13.40	8.17	13.29	13.30	20.25	10.72
	0.5	10.59	10.60	15.24	8.87	14.30	14.31	22.09	11.42
12	0	32.57	32.58	53.37	24.86	55.95	55.96	96.55	40.89
	0.1	32.63	32.64	53.48	24.90	56.01	56.02	96.65	40.93
	0.5	34.00	34.02	56.02	25.85	57.38	57.40	99.19	41.88

Fig. 2 depicts the pull-in voltage parameter of the *FG-X* SWCNTs reinforced piezoelectric polymeric nanocomposite plate against gap distance (g_0) for CT, MCST and MSGT. It is assumed that $a_3 = 0, a_4 = 0, a_5 = 0$ and $a_6 = 0$. As it shown, with an increase in the gap, distance decreases the pull-in voltage parameter also due to neglecting of rotational effects in classic plate theory, the CT and MCST results are very closer together. Furthermore considering the length scale parameter (l in MSGT) leads the nanocomposite plate becomes more inflexible.

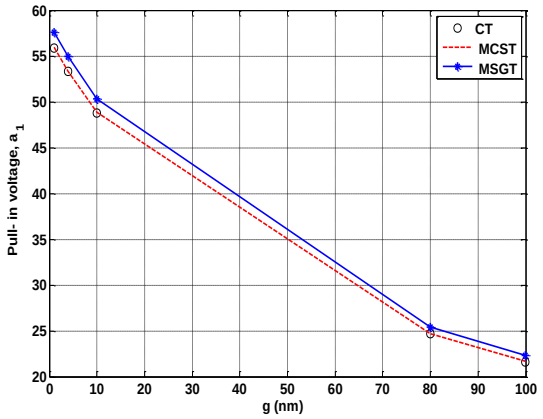

Fig.2
The pull-in voltage parameter of the FG-X SWCNTs reinforced piezoelectric polymeric nanocomposite plate against gap distance.

The pull-in voltage parameter of the FG-X SWCNTs reinforced piezoelectric polymeric nanocomposite plate versus magnetic field is demonstrated in Fig. 3. It can be seen that the pull-in voltage parameter increases with an increase in magnetic field because, when the magnetic field applied on the piezoelectric polymeric nanocomposite plate, the in-plane compression loads are emerged which enhances its stiffness therefore the pull-in voltage parameter increases. In addition, magnetic field effect on the pull-in voltage parameter in MSGT is higher than that of in CT and MCST.

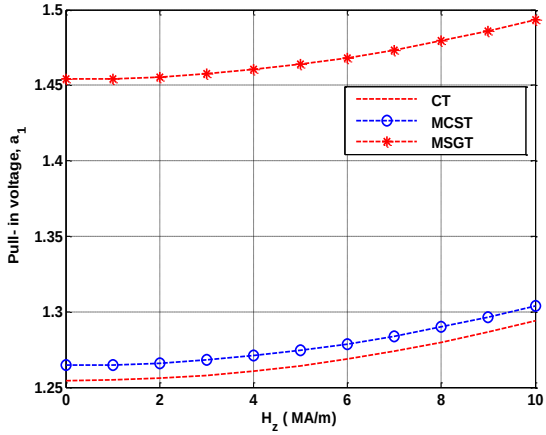

Fig.3
Magnetic field effect on the pull-in voltage parameter of the *FG-O* SWCNTs reinforced piezoelectric polymeric nanocomposite plate.

Effect of applied voltage on the pull-in voltage parameter of the *FG-O* SWCNTs reinforced piezoelectric polymeric nanocomposite plate is illustrated in Fig. 4. It is observed that the pull-in voltage parameter increases with increasing of the applied voltage. As the external voltage applied to the piezoelectric polymeric nanocomposite plate, it leads to increase stiffness of system.

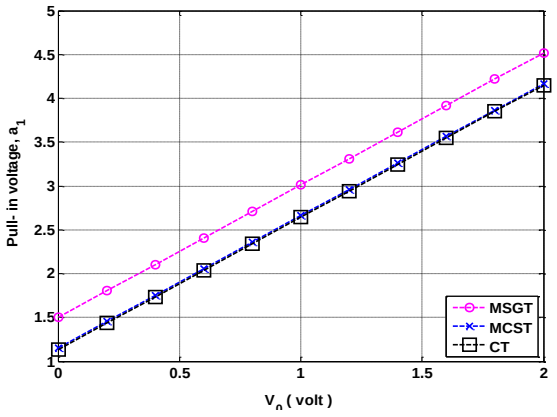

Fig.4
Applied voltage effect on the pull-in voltage parameter of the *FG-O* SWCNTs reinforced piezoelectric polymeric nanocomposite plate.

Fig. 5 displays effects of non-dimensional intermolecular forces, Casimir ($a_4 = r\pi^2 hcb/240g_0^5$) and van der Waals force ($a_3 = sAb/6g_0^4$) parameters on the pull-in voltage parameter of the *FG-O* SWCNTs reinforced piezoelectric polymeric nanocomposite plate for three small scale theories. It is clear in Fig. 5 that as these non-dimensional forces increases, the pull-in voltage parameter decreases particularly in MCST and MSGT. It is due to that interaction between atoms and molecules increases with increasing of these non-dimensional parameters. On the other hands, the stability of the piezoelectric polymeric nanocomposite plate decreases, therefore its pull-in voltage parameter decreases. Moreover, reduction effect of these parameters on the pull-in voltage parameter in MSGT is greater than other theories.

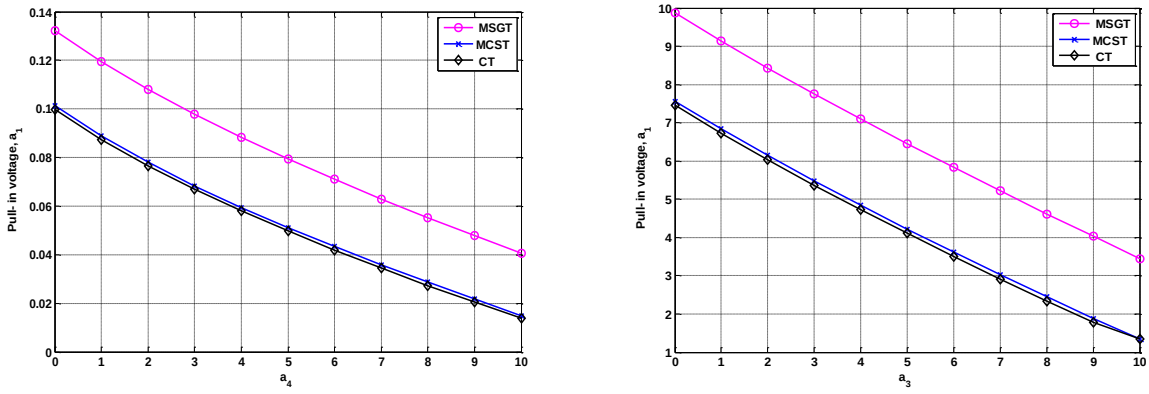

(a) (b)

Fig.5
The pull-in voltage parameter of the *FG-O* SWCNTs reinforced piezoelectric polymeric nanocomposite plate with respect to (a) non-dimensional Casimir force and (b) non-dimensional van der Waals force.

Surface stress effects (residual surface stress (τ_s) and Lame surface (E_s) constants) on the pull-in voltage parameter of the *FG-O* SWCNTs reinforced piezoelectric polymeric nanocomposite plate is illustrated in Figs. 6 and 7, respectively. As it can be observed from these figures that the pull-in voltage parameter decreases with an increase in residual surface stress. This means that surface stress creates a traction on surfaces of the piezoelectric polymeric nanocomposite plate which lead to its instability of nanocomposite plate occurs in lower pull-in voltage. But effect of Lame surface constant on the pull-in voltage parameter is negligible.

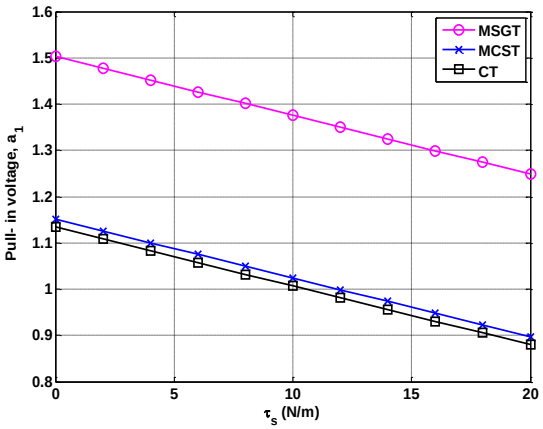

Fig.6
The pull-in voltage parameter of the *FG-O* SWCNTs reinforced piezoelectric polymeric nanocomposite plate with respect to residual surface stress constant.

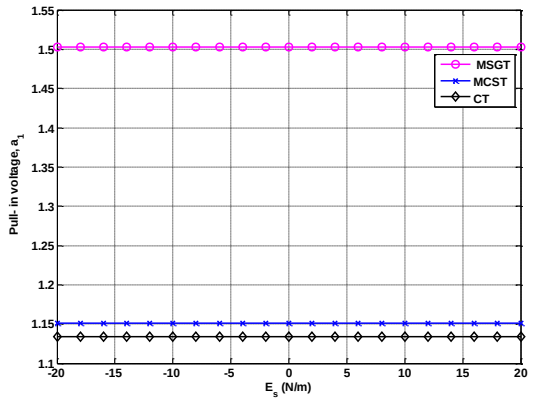

Fig.7
The pull-in voltage parameter of the *FG-O* SWCNTs reinforced piezoelectric polymeric nanocomposite plate with respect to Lame surface constant.

Fig. 8 shows the pull-in voltage parameter of *FG-X* SWCNTs reinforced piezoelectric polymeric nanocomposite plate against SWCNTs orientation angle (θ) based on MSGT. As it can be seen, the minimum of the pull in voltage parameter occurs in $\theta = \pi/2$.

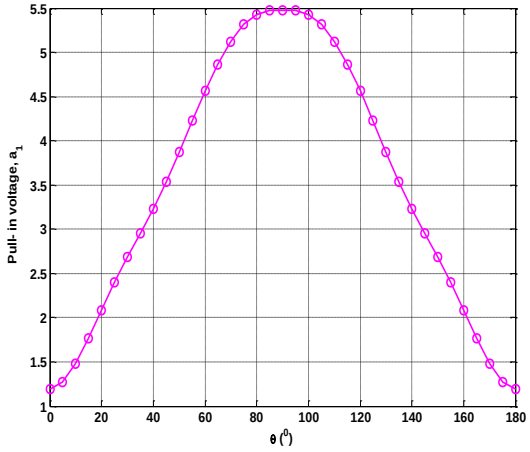

Fig.8
The pull-in voltage parameter of the SWCNTs reinforced piezoelectric polymeric nanocomposite plate with respect to SWCNTs orientation angle.

The natural frequency of the *UD*-SWCNTs reinforced piezoelectric polymeric nanocomposite plate against the pull-in voltage parameter for different non-dimensional van der Waals parameter (a_3) based on MSGT is depicted in Fig. 9. As it is displayed, the natural frequency decreases with increasing of the pull-in voltage parameter. Also in presence of van der Waals parameter, the natural frequency reduces.

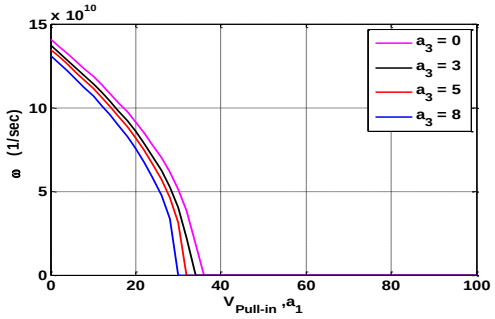

Fig.9
The natural frequency of the SWCNTs reinforced piezoelectric polymeric nanocomposite plate versus the pull-in voltage parameter.

The natural frequency of the SWCNTs reinforced piezoelectric polymeric nanocomposite plate with respect to the pull-in voltage parameter for various distributions of SWCNTs based on MSGT is shown in Fig. 10. As it is expected, the natural frequency in *FG-X* and *FG-O* distribution types are highest and lowest, respectively. The natural frequency of *UD* and *FG-V* distribution types are very closer together.

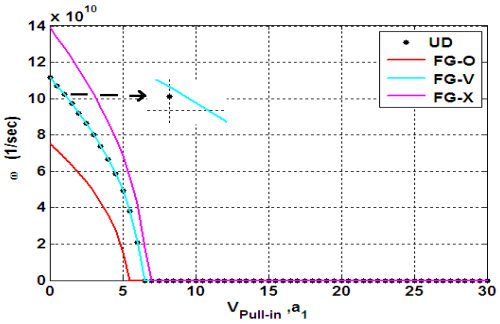

Fig.10
The natural frequency of the piezoelectric polymeric nanocomposite plate with respect to the pull-in voltage parameter for various distribution types of SWCNTs.

Residual, Lame surface stress and surface density effects on the natural frequency of the FG-X SWCNTs reinforced piezoelectric polymeric nanocomposite plate based on MSGT are displayed in Figs. 11, 12 and 13. As it is mentioned in the pull-in voltage parameter, increasing of residual surface constant decreases the natural frequency. But Lame surface constant hasn't any significant effect on the natural frequency. In addition, the natural frequency increases with increasing of surface density constant.

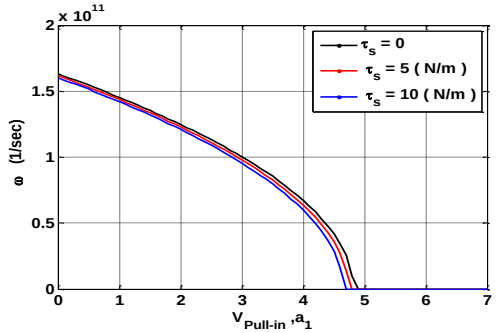

Fig.11
Effect of residual surface constant on the natural frequency of the *FG-X* SWCNTs reinforced piezoelectric polymeric nanocomposite plate.

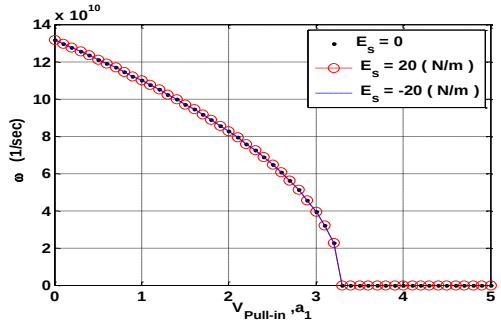

Fig.12
Effect of Lame surface constant on the natural frequency of the *FG-X* SWCNTs reinforced piezoelectric polymeric nanocomposite plate.

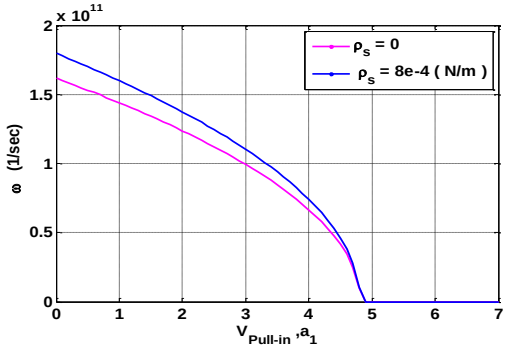

Fig.13
Effect of surface density on the natural frequency of the *FG-X* SWCNTs reinforced piezoelectric polymeric nanocomposite plate.

6 CONCLUSIONS

The pull-in instability of the *FG*- SWCNTs reinforced piezoelectric polymeric nanocomposite plate based on CT, MCST and MSGT was developed. Various types of SWCNTs were distributed in piezoelectric polymeric plate and surface stress effect was considered. The piezoelectric polymeric nanocomposite plate was subjected to electro-magneto-mechanical loadings. Governing equations were derived using Hamilton's principle. The nonlinear term was converted to linear term using Taylor expansion for the pull-in instability of nanocomposite plate. The pull-in voltage was obtained by Newton-Raphson method then the natural frequency was calculated. The following remarkable results are obtained as follows:

1. The MSGT pull-in voltage and natural frequency are greater than CT and MCST pull-in voltage and natural frequency.
2. Highest and lowest pull-in voltages are belonging to *FG-O* and *FG-X* distribution types of SWCNTs, respectively.
3. Casimir and Van der Waals forces have reduction effects on the pull-in voltage and the natural frequency.
4. The pull-in voltage and the natural frequency decrease with increasing of residual surface stress constant.
5. The pull-in voltage and the natural frequency increase with an increase in small-scale parameters.
6. The pull-in voltage increases with increasing of applied voltage and magnetic field.
7. The pull-in voltage for biaxial compression loading rather is more than that of for uniaxial compression loading.

ACKNOWLEDGMENTS

The authors would like to thank the Iranian National Science Foundation for their financial support.

REFERENCES

[1] Rocha L.A., Mol L., Wolffenbuttel R.F., Lage A., 2008, A time based micro- accelerometer, *Proceeding of Eurossensors XXII,* Dresden, Germany.

[2] Degani O., Nemirovsky Y., 2002, Design considerations of rectangular electrostatic torsion actuators based on new analytical pull-in expressions, *Journal of Microelectromechanical Systems* **11**(1): 20-26.

[3] Degani O., Socher E., Lipson A., Leitner T., Setter D.J., Kaldor S., Nemirovsky Y., 1998, Pull-in study of an electrostatic torsion microactuator, *Journal of Microelectromechanical Systems* **7**(4): 373-379.

[4] Zhang L.X., Zhao Y.P., 2003, Electromechanical model of RF MEMS switches, *Microsystem Technologies* **9**: 420-426.

[5] Senturia S.D., 2001, *Microsystem Design*, Boston, MA: Kluwer Academic.

[6] Koumela A., Mercier D., Marcoux C., Purcell S.T., 2012, Performances of suspended silicon nanowire resonators for time reference applications, *Proceedings of IEEE International Frequency Control Symposium,* Baltimore, MD, USA.

[7] Hassani F.A., Cobianu C., Armini S., Petrescu V., Merken P., Tsamados D., Ionescu A.M., Tsuchiya Y., Mizuta H., 2011, Numerical analysis of zeptogram/Hz-level mass responsivity for in-plane resonant nano-electro-mechanical sensors, *Microelectronic Engineering* **88**: 2879-2884.

[8] Colinet E., Durand C., Duraffourg L., Audebert P., Dumas G., Casset F., Ollier E., Ancey P., Carpentier J.F., Buchaillot L., Ionescu A.M., 2009, Ultra-sensitive capacitive detection based on SGMOSFET compatible with front-end CMOS process, *IEEE Journal of Solid-State Circuits* **44**: 247-257.

[9] Fu Y., Zhang J., 2011, Size-dependent pull-in phenomena in electrically actuated nanobeams incorporating surface energies, *Applied Mathematical Modelling* **35**: 941-951.

[10] Mohammadimehr M., Mohandes M., Moradi M., 2016, Size dependent effect on the buckling and vibration analysis of double-bonded nanocomposite piezoelectric plate reinforced by boron nitride nanotube based on modified couple stress theory, *Journal of Vibration and Control* **22**(7): 1790-1807.

[11] Wang Y.G., Lin W.H., Feng Z.J., Li X.M., 2012, Characterization of extensional multi-layer microbeams in pull-in phenomenon and vibrations, *International Journal of Mechanical Sciences* **54**: 225-233.

[12] Stephan D.A., Hannot Daniel J.R., 2013, A palette of methods for computing pull-in curves for numerical models of Microsystems, *Finite Elements in Analysis and Design* **67**: 76-90.

[13] Rudolf H.R.J., Seethaler A.S., Hosseini-Hashemi M., Li X.F., 2013, Analytical closed-form solutions for size-dependent static pull-in behavior in electrostatic micro-actuators via Fredholm integral equation, *Sensors and Actuators A: Physical* **190**: 32-43.

[14] Duan J.S., Rach R., Wazwaz A.M., 2013, Solution of the model of beam-type micro- and nano-scale electrostatic actuators by a new modified Adomian decomposition method for nonlinear boundary value problems, *International Journal of Non-Linear Mechanics* **49**: 159-169.

[15] Mousavi T., Bornassi S., Haddadpour H., 2013, The effect of small scale on the pull-in instability of nano-switches using DQM, *International Journal of Solids and Structures* **50**: 1193-1202.

[16] Sedighi H.M., Daneshmand F., Zare J., 2014, The influence of dispersion forces on the dynamic pull-in behavior of vibrating nano-cantilever based NEMS including fringing field effect, *Archives of Civil and Mechanical Engineering* **14**: 766-775.

[17] Wang K.F., Wang B.L., 2014, Influence of surface energy on the non-linear pull-in instability of nano-switches, *International Journal of Non-Linear Mechanics* **59**: 69-75.

[18] Fakhrabadi M.M.S., Rastgoo A., Ahmadian M.T., 2014, Non-linear behaviors of carbon nanotubes under electrostatic actuation based on strain gradient theory, *International Journal of Non-Linear Mechanics* **67**: 236-244.

[19] Yazdanpanahi E., Noghrehabadi A., Ghalambaz M., 2014, Pull-in instability of electrostatic doubly clamped nanoactuators: Introduction of a balanced liquid layer (BLL), *International Journal of Non-Linear Mechanics* **58**: 128-138.

[20] Askari A.R., Tahani M., 2015, Size-dependent dynamic pull-in analysis of beam-type MEMS under mechanical shock based on the modified couple stress theory, *Applied Mathematical Modelling* **39**: 934-946.

[21] Mojahedi M., Ahmadian M.T., Firoozbakhsh K., 2014, The influence of the intermolecular surface forces on the static deflection and pull-in instability of the micro/nano cantilever gyroscopes, *Composite Part B* **56**: 336-343.

[22] Jia X.L., Zhang S.M., Ke L.L., Yang J., Kitipornchai S., 2014, Thermal effect on the pull-in instability of functionally graded micro-beams subjected to electrical actuation, *Composite Structure* **116**: 136-146.

[23] Juillard J., 2015, Analysis of resonant pull-in of micro- electromechanical oscillators, *Journal of Sound and Vibration* **350**: 123-139.

[24] Huang Y.T., Chen H.L., Hsu W., 2014, An analytical model for calculating the pull-in voltage of micro cantilever beams subjected to tilted and curled effects, *Microelectronic Engineering* **125**: 73-77.

[25] Wang K.F., Kitamura T., Wang B., 2015, Nonlinear pull-in instability and free vibration of micro/nanoscale plates with surface energy- a modified couple stress theory model, *International Journal of Mechanical Sciences* **99**: 288-296.

[26] Rahaeifard M., Ahmadian M.T., 2015, On pull-in instabilities of microcantilevers, *International Journal of Engineering Science* **87**: 23-31.

[27] Shaat M., Abdelkefi A., 2015, Pull-in instability of multi-phase nanocrystalline silicon beams under distributed electrostatic force, *International Journal of Engineering Science* **90**: 58-75.

[28] Xiao Y., Wang B., Zhou S., 2015, Pull-in voltage analysis of electrostatically actuated MEMS with piezoelectric layers: A size-dependent model, *Mechanics Research Communications* **66**: 7-14.

[29] Moghimi Zand M., 2012, The dynamic pull-in instability and snap-through behavior of initially curved microbeams, *Mechanics of Advanced Materials and Structures* **19**: 485-491.

[30] Ghorbanpour Arani A., Jalilvand A., Ghaffari M., Talebi Mazraehshahi M., Kolahchi R., Roudbari M.A., Amir S., 2014, Nonlinear pull-in instability of boron nitride nano-switches considering electrostatic and Casimir forces, *Scientia Iranica F* **21**(3): 1183-1196.

[31] Ghorbanpour Arani A., Ghaffari M., Jalilvan A., Kolahchi R., 2013, Nonlinear nonlocal pull-in instability of boron nitride nanoswitch, *Acta Mechanica* **224**: 3005-3019.

[32] Lin S.M., Lee S.J., 2016, Coupled mechanism and pull-in instability of several probe-membrane assemblies subjected to electrostatic force, *Mechanics of Advanced Materials and Structures* **25**: 267-278.

[33] Yang W.D., Wang X., Fang C.Q., Lu G., 2014, Electromechanical coupling characteristics of carbon nanotube reinforced cantilever nano-actuator, *Sensors and Actuators A: Physical* **220**: 178-187.

[34] Tajalli S.A., Moghimi Zand M., Ahmadian M.T., 2009, Effect of geometric nonlinearity on dynamic pull-in behavior of coupled-domain microstructures based on classical and shear deformation plate theories, *European Journal of Mechanics A/Solids* **28**: 916-925.

[35] Fakhrabadi M.M.S., Rastgoo A., Ahmadian M.T., 2014, On the pull-in instability of double-walled carbon nanotube-based nano electromechanical systems with cross-linked walls, Fullerenes, *Nanotubes and Carbon Nanostructures* **23**: 300-314.

[36] Keivani M., Mokhtari J., Kanani A., Abadian N., Rach R., Abadyan M., 2016, A size-dependent model for instability analysis of paddle-type and double-sided NEMS measurement sensors in the presence of centrifugal force, *Mechanics of Advanced Materials and Structures* **24**: 809-819.

[37] Talebian S., Rezazadeh G., Toosi F.B.M., 2010, Effect of temperature on pull-in voltage and natural frequency of an electrostatically actuated microplate, *Mechatronics* **20**: 666-673.

[38] Zheng J.J., Dai J.G., 2014, Prediction of the nonlinear pull-out response of FRP ground anchors using an analytical transfer matrix method, *Engineering Structures* **81**: 377-385.

[39] Mohammadimehr M., Salemi M., 2014, Bending and buckling analysis of functionally graded Mindlin nano-plate model based on strain gradient elasticity theory, *Indian Journal of Scientific Research* **2**: 587-598.

[40] Ansari R., Gholami R., FaghihShojaei M., Mohammadi V., Sahmani S., 2014, Surface stress effect on the pull-in instability of circular nanoplates, *Acta Astronautica* **102**: 140-150.

[41] Ansari R., Mohammadi V., Faghih M., Shojaei R., Gholami M.A., Darabi A., 2014, Geometrically non-linear plate model including surface stress effect for the pull-in instability analysis of rectangular nanoplates under hydrostatic and electrostatic actuations, *International Journal of Non-Linear Mechanics* **67**: 16-26.

[42] Mohammadimehr M., Rousta Navi B., Ghorbanpour Arani A., 2015, Free vibration of viscoelastic double-bonded polymeric nanocomposite plates reinforced by FG-SWCNTs using MSGT, sinusoidal shear deformation theory and meshless method, *Composite Structure* **131**: 654-671.

[43] Mao R., Lu G., Wang Z., Zhao L., 2016, Large deflection behavior of circular sandwich plates with metal foam-core, *European Journal of Mechanics A/Solids* **55**: 57-66.

[44] Ghorbanpour Arani A., Rousta Navi B., Mohammadimehr M., 2015, Surface stress and agglomeration effects on nonlocal biaxial buckling polymeric nanocomposite plate reinforced by CNT using various approaches, *Advanced Composite Matererial* **220**: 1-19.

[45] Ghorbanpour Arani A., Khoddami Maraghi Z., Khani Arani H., 2016, smart vibration control of magnetostrictive nano-plate using nonlocal continuum theory, *Journal of Solid Mechanics* **8**(2): 300-314.

[46] Mohammadimehr M., Rousta Navi B., Ghorbanpour Arani A., 2015, Surface stress effect on the nonlocal biaxial buckling and bending analysis of polymeric piezoelectric nanoplate reinforced by cnt using eshelby-mori-tanaka approach, *Journal of Solid Mechanics* **7**(2): 173-190.

[47] Shojaeian M., Zeighampour H., 2016, Size dependent pull-in behavior of functionally graded sandwich nanobridges using higher order shear deformation theory, *Composite Structures* **143**: 117-129.

[48] Yang W.D., Wang X., Fang C.Q., 2015, Pull-in instability of carbon nanotube-reinforced nano-switches considering scale, surface and thermal effects, *Composites Part B* **82**: 143-151.

[49] Mohammadimehr M., Rousta Navi B., Ghorbanpour Arani A., 2017, Dynamic stability of modified strain gradient theory sinusoidal viscoelastic piezoelectric polymeric functionally graded single-walled carbon nanotubes reinforced nanocomposite plate considering surface stress and agglomeration effects under hydro-thermo-electro-magneto-mechanical loadings, *Mechanics of Advanced Materials and Structures* **24**: 1325-1342.

[50] Alibeigloo A., 2014, Free vibration analysis of functionally graded carbon nanotube-reinforced composite cylindrical panel embedded in piezoelectric layers by using theory of elasticity, *European Journal of Mechanics A/Solids* **44**: 104-115.

[51] Sedighi H.M., Bozorgmehri A., 2016, Dynamic instability analysis of doubly clamped cylindrical nanowires in the presence of Casimir attraction and surface effects using modified couple stress theory, *Acta Mechanica* **227**: 1575-1591.

[52] Hosseini S.A.H., Rahmani O., 2017, Exact solution for axial and transverse dynamic response of functionally graded nanobeam under moving constant load based on nonlocal elasticity theory, Meccanica **52**(6): 1441-1457.

[53] Malikan M., 2017, Analytical predictions for the buckling of a nanoplate subjected to non-uniform compression based on the four-variable plate theory, *Journal of Applied Computational Mechanics* **3**(3): 218-228.

[54] Ghorbanpour Arani A., Kolahchi R., Jamali M., Mosayyebi M., Alinaghian I., 2017, Dynamic instability of visco-SWCNTs conveying pulsating fluid based on sinusoidal surface couple stress theory, *Journal of Solid Mechanics* **9**(2): 225-238.

[55] Amiri A., Rezazadeh G., Shabani R., Khanchehgardan A., 2016, On the stability of an electrostatically-actuated functionally graded magneto-electro-elastic micro- beams under magneto-electric conditions, *Journal of Solid Mechanics* **8**(4): 756-772.

[56] Shaat M., Abdelkefi A., 2016, Size dependent and micromechanical modeling of strain gradient-based nanoparticle composite plates with surface elasticity, *European Journal of Mechanics-A/Solids* **58**: 54-68.

[57] Shaat M., Mahmoud F., Alshorbagy A., Alieldin S., 2013, Bending analysis of ultra-thin functionally graded Mindlin plates incorporating surface energy effects, *International Journal of Mechanical Sciences* **75**: 223-232.

[58] Shaat M., Mahmoud F., Gao X.L., Faheem A.F., 2014, Size-dependent bending analysis of Kirchhoff nano-plates based on a modified couple-stress theory including surface effects, *International Journal of Mechanical Sciences* **79**: 31-37.

[59] Ansari R., Ashrafi M., Pourashraf T., Sahmani S., 2015, Vibration and buckling characteristics of functionally graded nanoplates subjected to thermal loading based on surface elasticity theory, *Acta Astronautica* **109**: 42-51.

[60] Ansari R., Gholami R., 2016, Size-dependent modeling of the free vibration characteristics of post-buckled third-order shear deformable rectangular nano plates based on the surface stress elasticity theory, *Composites Part B: Engineering* **95**: 301-316.

[61] Batra R.C., Porfiri M., Spinello D., 2006, Capacitance estimate for electrostatically actuated narrow microbeams, *Micro & Nano Letters* **1**(2): 71-73.
[62] Israelachvili J.N., 2011, *Intermolecular and Surface Forces*, Academic Press, London.
[63] Lamoreaux S.K., 2005, The casimir force background, experiments, and applications, *Reports on Progress in Physics* **68**(1): 201-236.